

Calibration Properties of CHANDRA HETG Spectra Observed in CC-Mode

Norbert S. Schulz,¹ and the Chandra ACIS Calibration Team,^{1,2,3}
Version 3.0; Feb. 26, 2014

1. Introduction

The ACIS detector onboard Chandra offers two read out modes, Timed Event (TE) mode and Continuous Clocking (CC) mode. In TE mode events are accumulated for a specified amount of time (frame time; ft) and are collectively read out into a frame store buffer. Frame times can be set up to 10 seconds, the standard time for a full frame (1024 rows) is 3.2 seconds. This time can be reduced further through the creation of subarrays by limiting the number of rows. The lowest subarray size is 128 rows which corresponds to about 350 msec of frametime. In CC-mode events are read out continuously and here only the row by row readout time is relevant which amounts to 2.85 msec. It is higher than that for higher energy photons because framestore clocking has to be considered as well in order to determine the overall background. CC-mode is applied for various reasons, but its original dedication was to offer a fast readout mode.

Another application of CC-mode is for the mitigation of pile up in the charge coupled devices (CCDs) in bright sources. Photon intensities that exceed about 0.01 counts per pixel per frametime (cts/pix/ft) in a CCD cause events to pile up, i.e. there is a significant probability that the device cannot recognize two single photons and will register these at the sum of their energies. At low probability pileup fractions, this probability goes linearly with frametime and thus can be reduced by shorter frametimes. In timed event mode this is usually limited to the lowest standard subarray size and thus 350 msec for a single CCD. The best possibility in high intensity cases then is the application of CC-mode which reduces the incident flux rate over the full array by a factor $> 10^2$.

However the application of CC-mode comes at the expense of spatial information as any frame is collapsed into one row. We therefore do not find many bare ACIS observations, i.e.

¹Kavli Institute for Astrophysics and Space Research, Massachusetts Institute of Technology, Cambridge, MA 02139.

²Center for Astrophysics, Cambridge, MA 02139.

³Marshall Space Flight Center, Huntsville, AL.

CC-mode and no gratings, of high intensity objects in the Chandra archive. CC-mode is now primarily used in grating spectroscopy. Chandra has three grating types, low (LEG), medium (MEG), and high (HEG) energy gratings for high resolution spectroscopy in the bandpass from 0.3 to 8 keV at up to 1200 in spectral resolving power. The MEG and HEG gratings are mounted on the high energy transmission grating (HETG) support structure. The grating disperses X-ray energies into various orders through the dispersion equation. The zeroth order produces an X-ray image, higher orders disperse photons into MEG + HEG spectra which are simultaneously captured by the ACIS-S array. The array contains six CCD devices labeled from S0 to S5, with the zeroth order image on S3. The HETG itself also acts as a blocking filter for 0th order events because the grating facets are mounted on a few μm thick polyimide film, which reduces the flux to by an energy dependent factor of around 4.5 at 1 keV.

The dispersive property of the grating allows us to record proper X-ray spectra with source intensities of up to several tens of mCrab with the MEG and HEG using reduced frametimes through subarrays in TE-mode. Many bright Galactic plane and bulge sources and X-rays transients reach much higher fluxes and pileup in grating spectra can become a problem. Once the rate in pixels recording the dispersed photons enters the high-pileup probability regime, photons get redistributed from the 1st order into the higher orders. Even though advanced algorithms can fully model spectral continua under some circumstances, it is impossible to treat discrete line features without further modeling assumptions. Spectra in CC-mode are specifically useful as they remain pileup-free for basically all existing X-ray fluxes and preserve most line features. This, however, comes at the price that continuum information gets lost and/or our ability to calibrate and analyse broadband continua becomes highly limited.

In the following we describe fundamental properties of bright CC-mode X-ray spectra using the HETG and the ACIS-S detector array. Some emphasis is given on setting flux guidelines of when to use CC-mode. A description of specific properties of spectra as a consequence of collapsing the dispersed image, calibration deficiencies, and configuration guidelines for future observations is presented.

2. Calibration Sources

Most data sets used for this study come from the guest observer observation program or guaranteed time observations. In some cases we added a calibration follow-up observation in order to compare results from different configurations or instrument settings. Table 1 lists some relevant properties of some of the X-ray sources and instrument configurations.

4U1957+115 is one of the sources we observed in the calibration program in three parts consisting of a TE mode, CC-mode, and TE-mode in direct succession. It is the faintest of the sources in the calibration sample, but with 35 mCrab is just bright enough to allow TE mode observations with only little pile-up degradation.

TABLE 1 CALIBRATION SOURCE PROPERTIES

Sources	Obsids	Flux (1)	Flux (2)	N_H (3)	exposure (4)	Mode	Subarray	Z-Sim (5)
4U 1957+115	10659	35	0.80	0.15	10	TE	15, 440	-6.8
	10660		0.80	0.15	20	CC	–	-6.8
	10661		0.80	0.15	10	TE	15, 440	-6.8
4U 1728-34	2748	85	2.00	2,51	30	TE	1, 400	-7.49
	6567		2.00	2,51	160	CC	–	-4.0
GX 13+1	11817	330	7.94	3.16	30	TE	1, 350	-8.0
	11818		7.94	3.16	30	CC	faint	-8.0
	13197		7.94	3.16	10	CC	graded	-8.0
GX 349+2	12199	660	15.8	1.99	20	CC	–	-6.14
	13220		15.8	1.99	20	TE	1, 300	-11.3
	13221		15.8	1.99	40	CC	–	-6.14
Cyg X-2	8170	540	13.2	0.32	70	CC	–	-6.14
	8599		13.2	0.32	70	CC	–	-6.14
	10881	340	8.2	0.32	100	CC	–	-6.14
GX 5-1	5888	700	17.0	3.36	50	CC	–	-11.3

(1) [mCrab], (2) [$10^9 \text{ erg cm}^{-2} \text{ s}^{-1}$], (3) [10^{22} cm^{-2}], (4) [ks], (5) [mm]

Figure 1 shows images of the dispersed spectra on the ACIS-S array in TE mode. In CC mode there are no full images as the y-pixel scale is collapsed. The top panel shows 4U 1957-115 observed in a custom 440 row subarray mode which covers most of the source-relevant HETG bandpass. The middle panel shows the bright source GX 13+1 observed with a more restricted 350 row subarray and a bandpass limited to about 18 Å. The lower panel shows the even brighter source GX 349+2 in an even more restricted subarray but now with MEG -1st and HEG +1st orders out of the array. This further reduces HETG pileup but at the expense of reduced effective area and bandpass.

The question of when and how to use TE and CC-mode to obtain HETG spectra depends on instrumental settings and the basic properties of the expected spectrum. The dominating parameter is the incident source flux as it, sometimes in conjunction with photoelectric X-

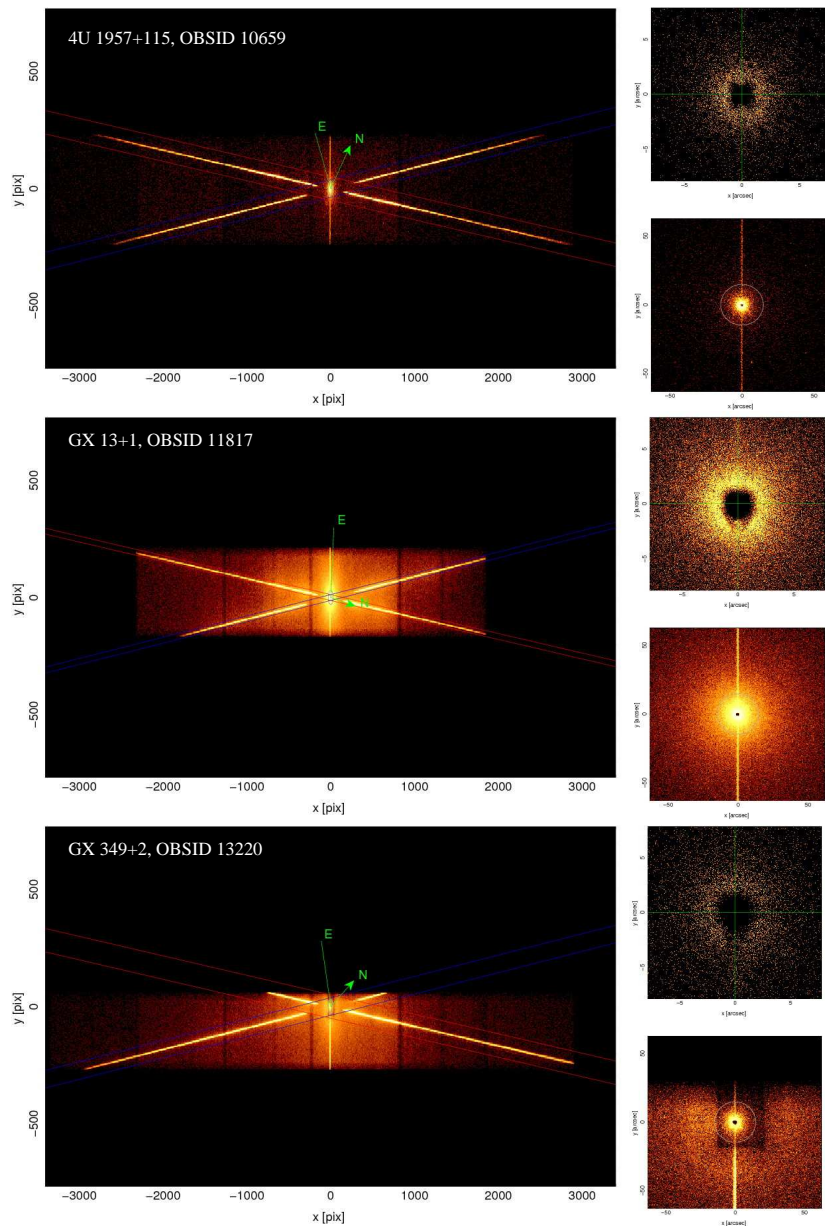


Fig. 1.— Three calibration sources observed in TE mode at different fluxes and configurations (see Table 1). The top shows the full dispersed image of obsid 10659 at a low flux. The two panels to the right show two zooms of the zero order image, which in this case indicates pileup blackouts at the center, but not much of a halo beyond the point spread function scatter. The middle and bottom panels show the same for obsid 11817 at a factor 10 higher flux, and obsid 13220 at a factor 20 higher flux. In the latter two grating arms have been placed off the CCD array and a transmission filter has been applied to the zero order image.

ray absorption, defines the choice of instrument settings. There are three main regimes to consider, which we simply refer to as low, medium, and high X-ray fluxes. These regimes have substantial overlaps which depend on the settings and desired spectral band pass.

2.1. Low Flux Regime (< 35 mCrab)

We consider any sources that can be safely observed in TE mode without the application of more restrictive subarrays (< 513 rows, > 1.7 sec frametime) part of the low flux regime. Here fluxes up to about 10 mCrab can be accommodated without pileup losses. However, as a standard mode for non-stellar fields, usually a 512 row subarray (< 1.7 sec frametime) starting at the readout row is applied. This allows for about 25 mCrab without pileup losses. About 35 mCrab may be possible by restricting the bandpass through shutting off devices, though in these cases different choices of subarrays are likely more effective. We have one calibration source in the low flux regime at about 35 mCrab, 4U 1957+115, which was observed in direct succession for 10 ks in TE mode, 20 ks in CC mode, and again for 10 ks in TE mode in order to exclude possible spectral variations between the TE and CC mode observations. We applied a 440 row subarray in TE mode which allowed for some pile-up ($< 6\%$) to affect the spectra.

2.2. Medium Flux Regime (< 350 mCrab)

In general the application of subarrays can accommodate fluxes up to about 350 mCrab, but with very restrictive bandpasses and the loss of effective area and manageable pile-up losses. In the most extreme case bandpasses can be limited to > 2 keV (< 6.2 Å), which corresponds to a 128 row subarray (~ 0.4 sec frametime) starting at the readout row and the operation of only two devices in the array. For practical reasons it is assumed that CC-mode is only used when deemed necessary and otherwise TE mode is always desired.

Table 1 contains two calibration sources in the medium regime: 4U 1728-34 at 85 mCrab, which has been observed in TE mode with a 400 row subarray for 30 ks, but also in CC-mode for 160 ks; GX 13+1 was observed several times since launch, here we chose two GTO observations, one in TE mode with a 350 row subarray, another one with the same SIM-Z setting in CC-mode. Another 10 ks calibration observation was added to verify the use of graded mode in CC-mode. Even though CC-mode spectra are calibrated as TE mode spectra, these calibrations have to be validated.

Note, the choice of TE versus CC mode also depends on the source spectrum. The

reason why GX 13+1, which at 330 mCrab is already extremely bright, could be observed in TE mode with only minor pileup losses ($< 10\%$) was because of its high X-ray absorption and relatively hard spectral properties, i.e. X-ray fluxes drop rapidly from 2 to 10 Å.

2.3. High Flux Regime (> 350 mCrab)

Most bright Galactic bulge sources, BH transients, some persistent LMXBs and HMXBs fall in to the high flux regime above 300 mCrab. For 95% of these cases it is strongly advised to use CC mode in order to preserve absorption and emission lines. However, there are many issues associated with the use of CC mode which are discussed in the following.

3. ACIS Calibration between TE and CC mode

In this section it is assumed that spectra in TE mode are sufficiently well calibrated to be used as a standard to compare with CC mode spectra. There are several issues we consider for calibration of the ACIS instrument. These are energy scale and gain, the ACIS response function, trailing charges from charge transfer inefficiency (CTI), and quantum efficiency and its uniformity. In the following we describe possible differences between TE and CC mode and its impact on the overall ACIS calibration in CC mode.

3.1. Energy Scale and Gain

The energy (wavelength) scale in HETG spectra is defined by the dispersion equation and primarily does not depend on the ACIS PHA's. It is relevant for event extraction of the spectra. The event extraction relies on the order sorting table (OSIP) which is a combination of spatial and pulse height extraction windows (see also Section *CTI Corrections*). Therefore in order to investigate differences between the behavior in TE and CC mode we need to look at the relative positions of the orders in pulse height (pha) space.

Figure 2 shows a slice in pha space of HETG spectral orders. In this case the pha's at 9.8 ± 0.3 Å are shown for the MEG $+1^{st}$ and HEG -1^{st} orders in three different configurations. The bright source GX 349+2 was observed in TE and CC mode in various configurations. It is bright enough to produce usable orders up to the 4th order. Anything higher likely stems from ACIS high energy CC-mode background in the OSIP extraction windows (see Sect. *CC-Mode Background*). The top and middle two panels show extractions from CC-mode configurations, the bottom two panels a TE mode observation of GX 349+2 with two grating

arms located off the array. This allows us to directly compare TE and CC-mode results on energy scale and gain. The statistics of the first order peaks allow a gain determination to $< 0.5\%$, close to the 0.3% standard from the external calibration source determinations in imaging data. The higher orders are fainter and only allow a gain determination of up to 3.0% , which is still sufficient for order sorting.

We determined first and higher order peaks at several wavelengths ranging from 2 to 18 \AA for all orders where available. The ratios of first to third order PHA peak positions showed variations less than 1.0% , and other orders showed variations less than 2.5% . There was no difference between CC and TE mode ratios of order peak positions. This shows that the energy scale in CC mode is not significantly different with that used in TE mode.

The same procedure was selectively repeated on the MEG -1^{st} and HEG $+1^{st}$ orders. While the ratios with the higher orders remained within the 3% accuracy of the measurement, the first order gain determinations were only good within $3 - 5\%$. While this is still not problematic with respect to order sorting, it shows that there is an issue with CTI (see Sect. CTI Correction) in CC-mode.

3.2. ACIS Response Function

In each ACIS device the response varies with increasing row number mainly due to increasing charge losses from CTI with distance to the readout. In back-illuminated (BI) devices there is also a dependence on pixel column due to serial CTI. In TE mode each device is sectioned into 32×32 pixel regions, which have their unique ACIS Response Matrix Files (RMFs). Generally at this stage the differences between neighboring RMF regions is small, significant effects, however, can be noted between more distant regions resulting in differences in spectral resolving powers of up to 50% from near the readout to farthest from the readout.

In CC-mode all rows with their various response properties are collapsed into one readout row. The result is a weighted average response across the entire device. However, there are two effects that mitigate the response blur in CC mode for HETG observations. The first relates to the fact that nearly all HETG observations are recorded close to the readout, i.e. within the first 512 rows. This means that the largest blur from the regions higher than row 512 get mapped into the cc-mode background only. This is because the ACIS response degrades with increasing number of rows. The second relates to the fact that wider cross-dispersion PHA distributions will still be accounted for by a fairly open order sorting table. In this respect the current application of ACIS responses, which is used to generate

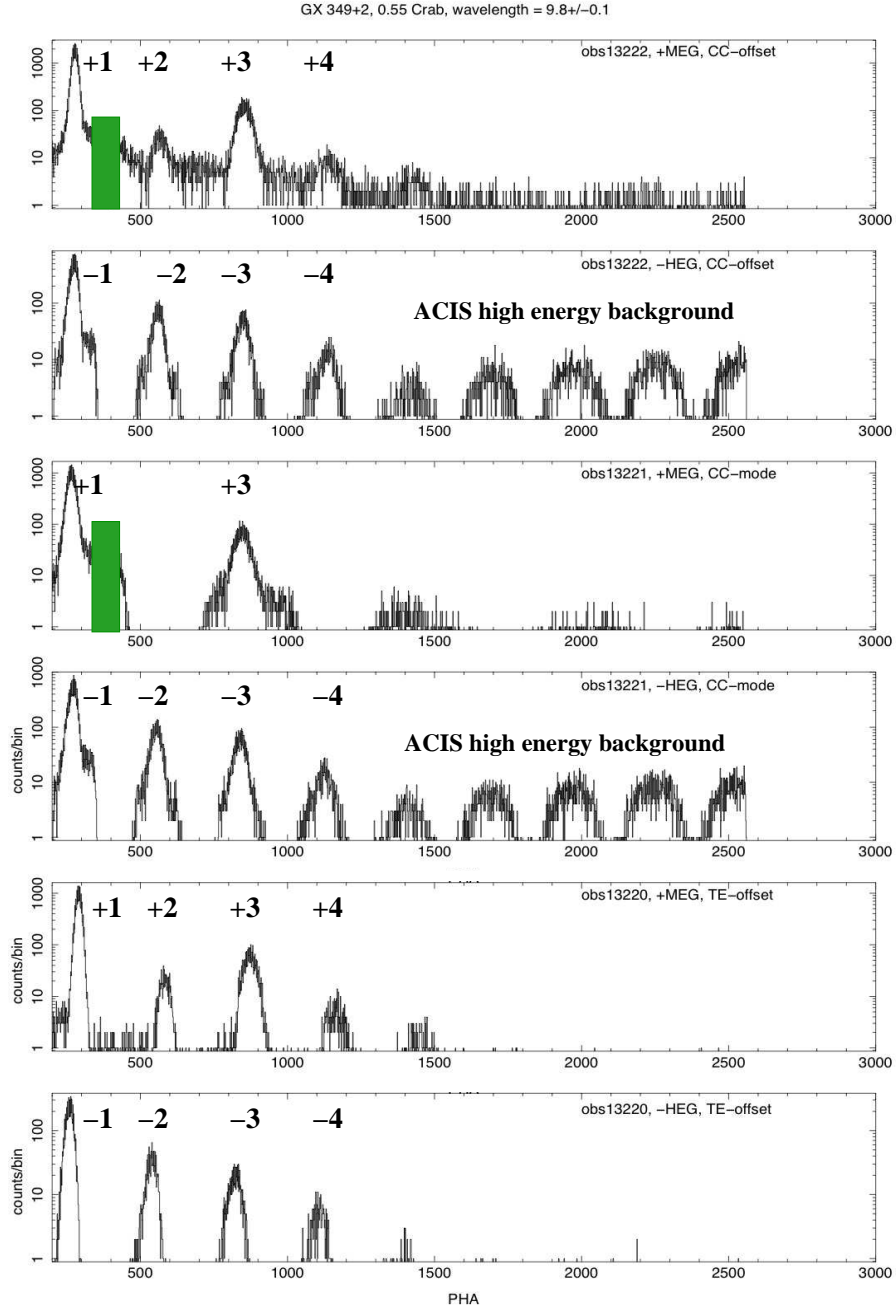


Fig. 2.— The order sorting in pha space at 9.8 Å in CC and TE mode in MEG +1st and HEG -1st order for different configurations as observed in GX 349+2 (see Table 1). The top two panels show the orders for the configuration with a Z-Sim offset of -11.3 mm in CC-mode, which puts two grating arms off the CCD array (see Figure 1, bottom). The middle two panels are the same source but with a Z-Sim offset of -6.14 mm and all grating arms on the CCD array. The bottom panel is the same source with a Z-Sim offset of -11.3 mm, but in TE-mode. The numbers mark the extracted orders. The green rectangles mark background extraction regions.

the grating order extraction, should have no significant effect on the HETG spectral quality. In BI devices we should encounter charge redistributions in dispersion direction in the 3x3 pixel island due to serial CTI which will be reflected in the grade distributions (see below).

3.3. CTI Correction

Each CCD in the ACIS-S array suffers from time-dependent CTI, which leaves charge trails in the PHA distribution which alter event recognition and allow events to drift out of the order sorting window. The CTI correction in TE mode is based on measured charge trap maps for each device and column to predict and properly correct for charge losses across the devices. In CC-mode charges are clocked continuously through the Si lattice which changes the trap charge distribution and trap release time scales. To date we have not found alternate trap maps for CC-mode that further improve corrections beyond the level achieved when using the TE-mode maps.

Figure 3 shows a comparison between energies computed from the dispersion relation and the ACIS detector gain for HETG events in the 1st orders. In a perfect world the events should scatter tightly and symmetrically around the first order sorting line marked in red. It shows that while the pipeline CTI correction in TE-mode observations aligns the resolved events very symmetrically around the order line. The one in CC-mode shows significant deviations. In most cases these deviations are not severe enough to affect order sorting in most of the available wavelength bands. Exceptions are likely to happen in the HEG +1st orders longward of 11 Å and the MEG -1st orders longward of 16 Å. The HEG -1st and MEG +1st orders seem very well constrained in CC-mode. The main reasons for this are likely the worse CTI on S5 in the case of the HEG +1st order and similarly on S1 for the MEG -1st order at low energies.

There are three strategies for performing and analyzing CC-mode HETG observations. The first is to primarily observe HEG -1st and MEG +1st orders only, which (see below) would also be a preferred solution for the HEG/MEG higher order background containment. For this one has to move the aimpoint beyond the readout row. The second would call for a custom OSIP, which however, due to the difficulties stemming from creating the OSIP tables from the ACIS responses, is very labor intensive. A third solution to improve the correction is to apply actual y-pix coordinates. The TE trap map application in CC-mode is currently very simplistic. Due to the lack of y-pix coordinates only the projected location of the zeroth order is used for the correction. This may be improved by one iterative step in which one actually calculates the dispersed y-pix coordinates for the entire tg_resolved HETG spectrum and applies that coordinate to a modified CTI correction. Figure 4 compares the result for

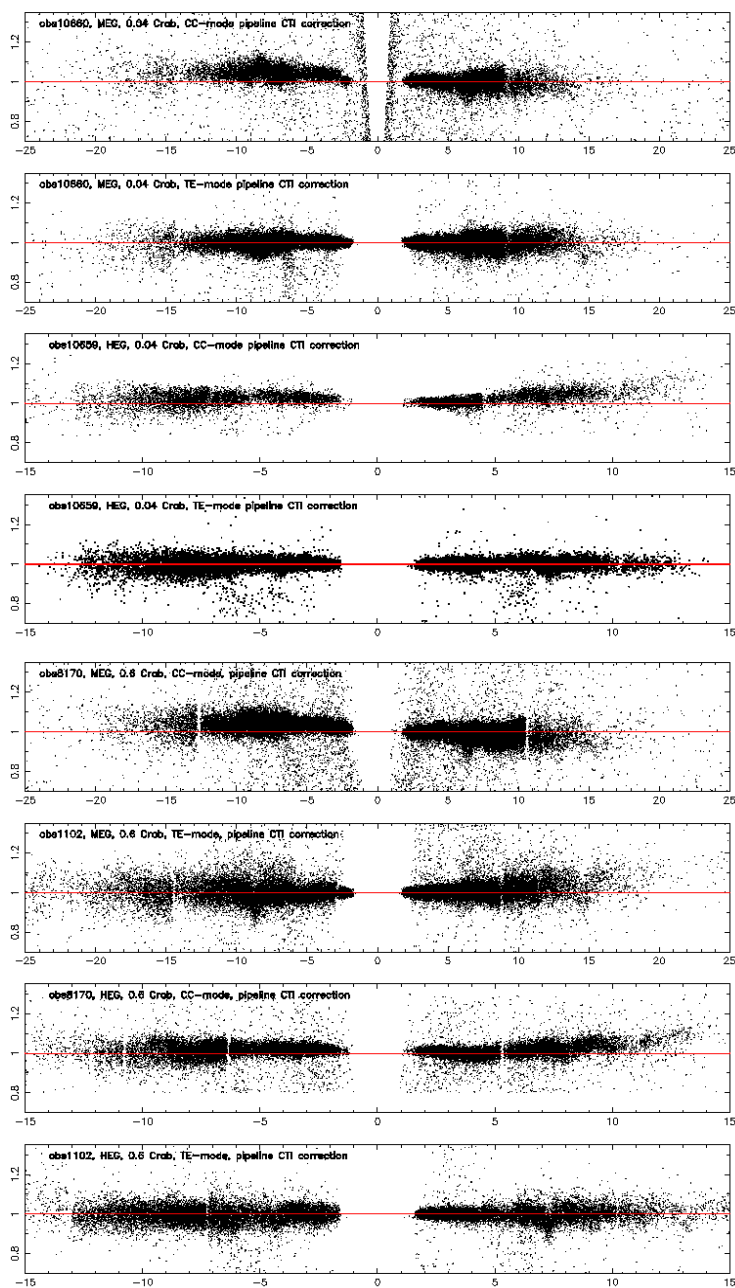


Fig. 3.— First order OSIP plots (+1st orders on the right side) using the first 10^5 events in the resolved event lists and first orders (y-scale) only. The x-scale is the tq_mlam order sorted wavelength column. The top four show the pipeline corrected MEG and HEG orders for CC-mode and TE mode for the 35 mCrab calibration source 4U1957-115, the bottom four panels show the same for the bright 0.6 Crab source Cyg X-2.

an observation of GX 13+1. The top three panels are MEG and the bottom three are HEG. This shows that the modified CTI correction is improved with respect to the pipeline correction when using the actual y-pix values for each event.

3.4. Grade Sets and Distributions

One of the largest differences between TE and CC-mode is the distribution of flight grades and how they map into the standard distribution of grades. The TE mode calibration is entirely based on the standard set of grades, which group the 256 flight grades into 8 grade categories of which three grade categories, 1, 5, and 7 are rejected and 0, 2, 3, 4, and 6 are accepted and called the standard grade set. The calibration is always based on the sum of the these standard grades. Figure 5 (top) shows the grade distributions for a TE mode observation (OBSID 10659) for the MEG -1st order covering devices S3, S2 and S1. In all chips grade 0 is the largest contributor followed by 2, 3 and 4, and 6. In S2 grades other than 0 grades only contribute about 20% to the total, while on S1 the contributions are higher. On S3 there is a grade swap in that grade 6 becomes the dominant grade. All these effects are known and are accounted for in the TE mode calibration. Figure 5 (center) shows the same source (obsid 10660) observed in CC-mode. On S1, i.e. longward of 14 Å, the grades distribute rather similar to the TE-mode case, grades 0 and 2 seem more equally distributed. The most prominent effect we observe is on S2, where shortward of about 10 Å grade 0 events rapidly decrease and grade 2 events become dominant. This is not unexpected since grade 2 corresponds to an event with trailing charge. There are two discrete features observed: one is identified as the Si K edge in grades 3,4 and 6 similar to the TE mode case, the other is a local drop at 8.2 Å in grades 0, 3, and 4, which seems to be compensated by an excess in grade 2 and which coincides with a CTI anomaly near the border of nodes 1 and 2 on S2. Even though there is a lot of detail in these distributions and many of these details are not well understood in TE and CC-mode, it is important how the integrated grade distributions compare. When we integrate all standard grades over the entire bandpass, the total X-ray flux between TE-mode and CC-mode agree within 2%. This is the same level of variation the source showed between the two TE mode observations which were 22 ksec apart with the CC-mode observation in between. Bin by bin variations of 0.06 Å bins between the TE and CC mode observation are limited to about 7% and appear random due to source statistics (see also Fig. 6, bottom panel).

Very bright sources are central to this CC-mode investigation and the question remains if the agreement between fluxes derived in CC- and TE-mode also holds for very bright sources. Figure 5 (bottom) shows the grade distributions for S2 and parts of S1 for the

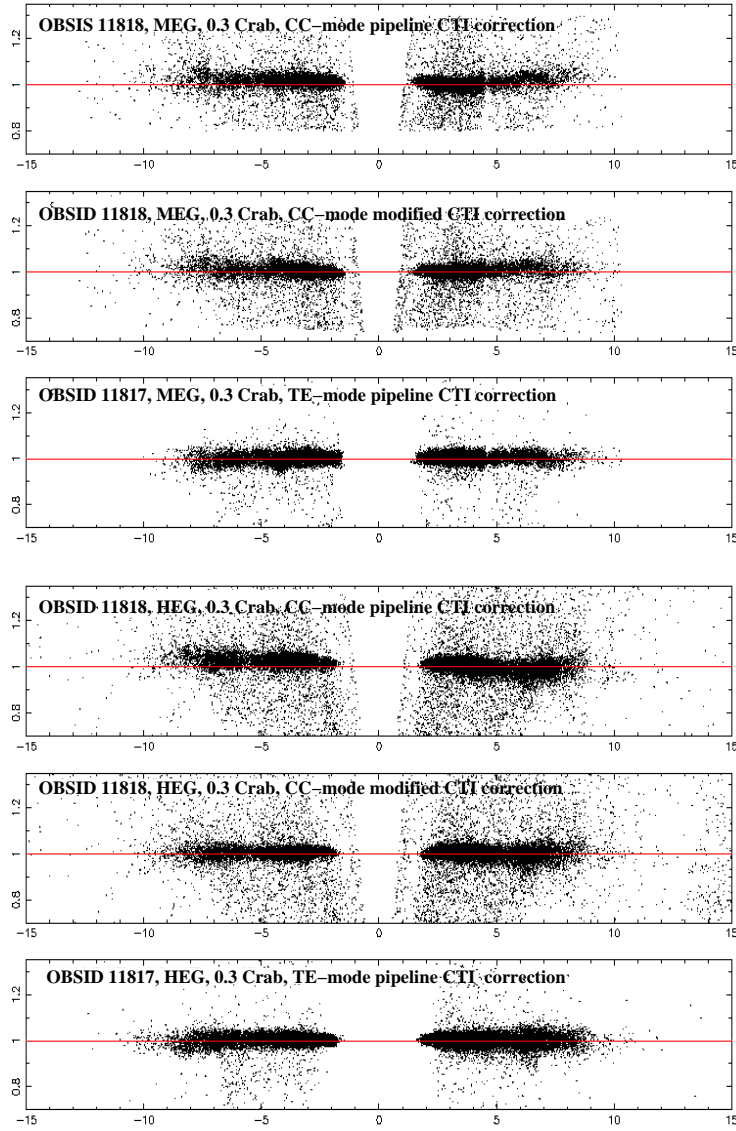


Fig. 4.— CTI correction as applied in CC mode for MEG (Top three panels) and HEG (bottom three panels) and compared to TE mode. For each grating the top panel shows the TE mode pipeline CTI correction to the CC mode spectra, the middle panel shows the resulting spectrum when the actual y-pix value is used for each event when applying the CTI correction, the bottom the pipeline CTI correction applied on TE mode spectra.

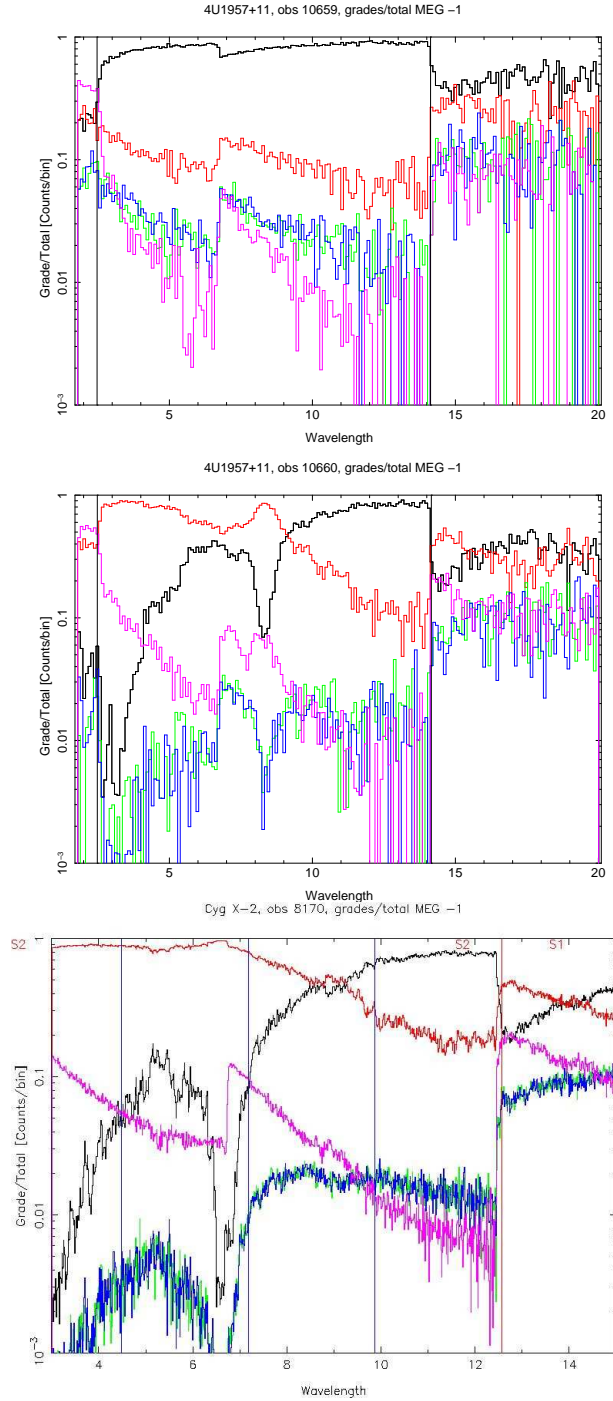


Fig. 5.— Grade distributions for 4U 1957-115 in TE (top) and CC (middle) mode at ~ 35 mCrab. The bottom panel show Cyg X-2 in CC mode at 540 mCrab. The colors are grade 0 (black), grade 2 (red), grade 3 (green), grade 4 (blue), and grade 6 (magenta).

case of Cyg X-2 (OBSID 8170) at 0.6 Crab. The observation had slightly different off-sets and comparable features with Figure 5 (center) appear at different wavelengths but still at similar locations on the CCD. It can be seen that the grade pattern with respect to CCD location between the low and high flux case are very similar indicating that the instrument response with respect to event detection and grade distribution is not significantly changing. We cannot make direct flux comparisons between the TE and CC-mode case because of heavy pileup in the TE-mode data (see sections below).

3.5. Faint vs. Graded Mode

Most observations of very bright sources use onboard pulse height summing (graded mode) in order to save space in the telemetry stream. In that case only the standard grade sets 0-7 are telemetered. Generally there should not be much difference between graded and faint mode spectra and for the few sources observed in both, CC-faint and CC-graded mode, we did not observe significant differences. However, by looking into the flight grades it has been noted that flight grade 66, which usually is part of the rejected grade set, shows some enhancement and tests reveal that shortward of 3 \AA the inclusion of this flight grade recovers up to a few percent of the flux in some cases. Since 2010 this grade and a few others are now part of the telemetry stream of graded CC-mode observations.

3.6. TE vs. CC Mode Spectra

The previous sections have shown that there are subtle differences between TE- and CC-mode. From the perspective of ACIS instrument calibration they can all be explained by the effects of CTI. In HETG spectra these differences have practically no effect as they are largely covered by the OSIP extraction process. This can be seen in our calibration source 4U 1957-115 (Fig. 6), where we have successive TE- and CC-mode spectral coverage and no intrinsic spectral variation between these observations. In general the CC-mode extractions of the four grating arms, MEG -1st order (black), MEG +1st order (red), HEG -1st order (green), HEG +1st order (blue), overlap well in both CC- and TE-mode. The match can be seen in the bottom panel which shows the corresponding ratio between the TE- and CC-mode spectra. Towards the soft end there is a slight difference of a few percent between the MEG and HEG, which is explained by a higher order overlap and which is addressed in Sect. *High Order Background* below.

The fact, however, that there are observed differences and problems in HETG CC-mode

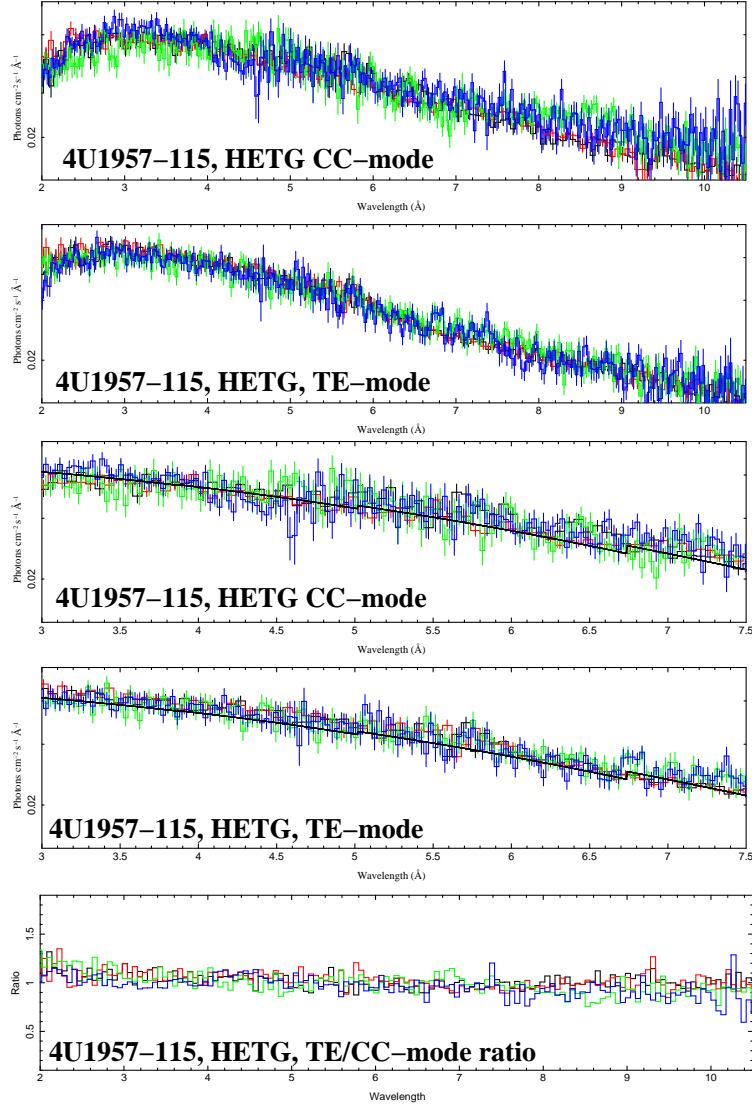


Fig. 6.— Comparison of HETG spectra for 4U 1957-115 in TE and CC mode at ~ 35 mCrab. The top two panels shows the the 2 - 10.5 Å bandpass, the middle two panels a blowup of the critical 3 - 7.5 Å bandpass. The bottom panel shows the ratio of TE over CC mode spectra for the four 1st orders. MEG -1st is black, MEG +1st is red, HEG -1st is green, and HEG +1st is blue.

spectra is demonstrated in Figures 7 and Figures 8. These are HETG spectra of bright X-ray binaries for a variety of fluxes, spectral shapes and absorption. While some cases show quite dramatic effects, such as in Cyg X-2, Cyg X-1, or GX 339-4, some others such as 4U 1630-47 are hardly affected at all. Most sources in these two figures have fluxes above 200 mCrab.

In the following we describe effects specifically affecting HETG spectra and possible fixes.

4. Why is CC mode different for HETG spectra

There is a major difference between TE- and CC-mode HETG spectra in the way they are recorded. While in TE-mode the dispersive imaging properties are completely preserved, in CC-mode one dimension is collapsed and this has severe consequences, specifically for sources with X-ray columns larger than 10^{21} cm⁻². In essence most CC-mode effects strongly depend on the source image and the incident source spectrum and are therefore predominantly science issues.

We have identified three major effects that can alter the extracted HETG spectra in CC-mode with respect to TE-mode:

- *Additional extended source dispersions:* this effect, is primarily caused by extended source emissions which also disperse and which are merged differently into each of the four HETG spectral arms. In bright absorbed X-ray binaries this results from a significant scattering halo in the source image. Another less significant feature originates from dispersion of the scattering tail of the psf, which in some cases can affect the cross-dispersion flux normalization.
- *High order background:* this affects HEG 1st order spectra from a direct overlap with MEG 2nd order spectra.
- *CC-mode (soft) background:* in CC-mode all 1024 rows of a device get clocked into each other enhancing any existing charge background accordingly.

5. The Scattering Halo in CC-mode

The primary effect we identified which can alter dispersed HETG spectra is the X-ray source's dust scattering halo present in brighter and more absorbed sources. Figure 9 shows five examples of HETG images including the zero order image. The bottom panel shows our

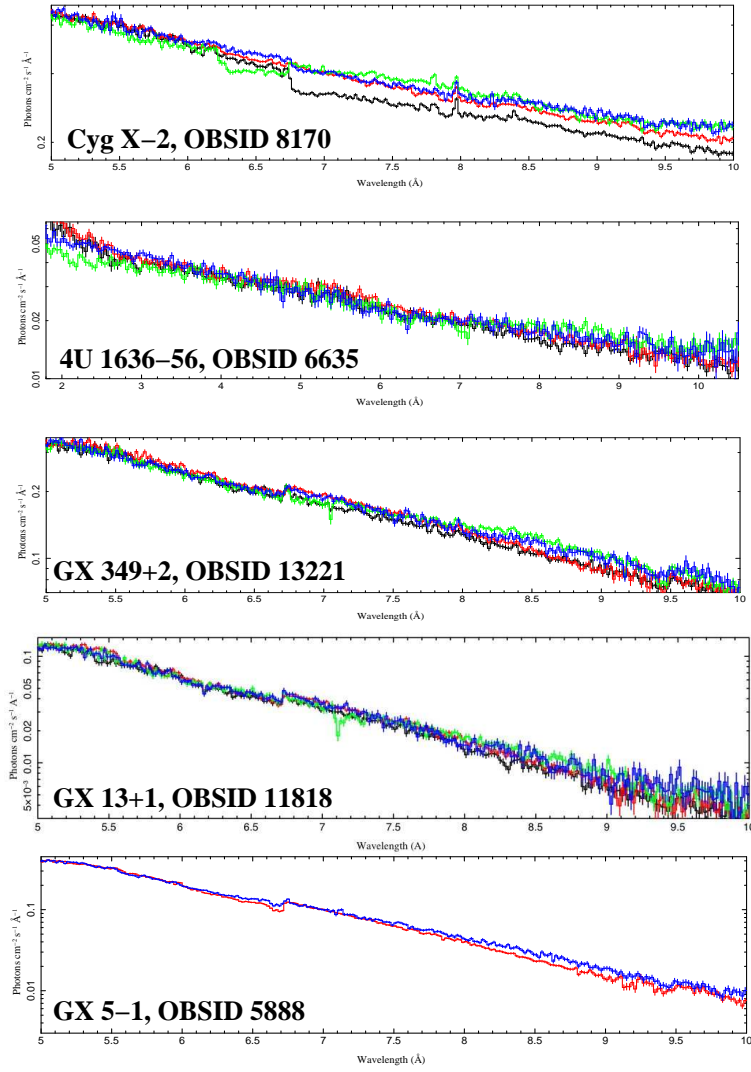


Fig. 7.— Various CC-mode HETG spectra for for bright LMXBs above 50 mCrab and various spectral shapes. MEG -1st is black, MEG +1st is red, HEG -1st is green, and HEG +1st is blue.

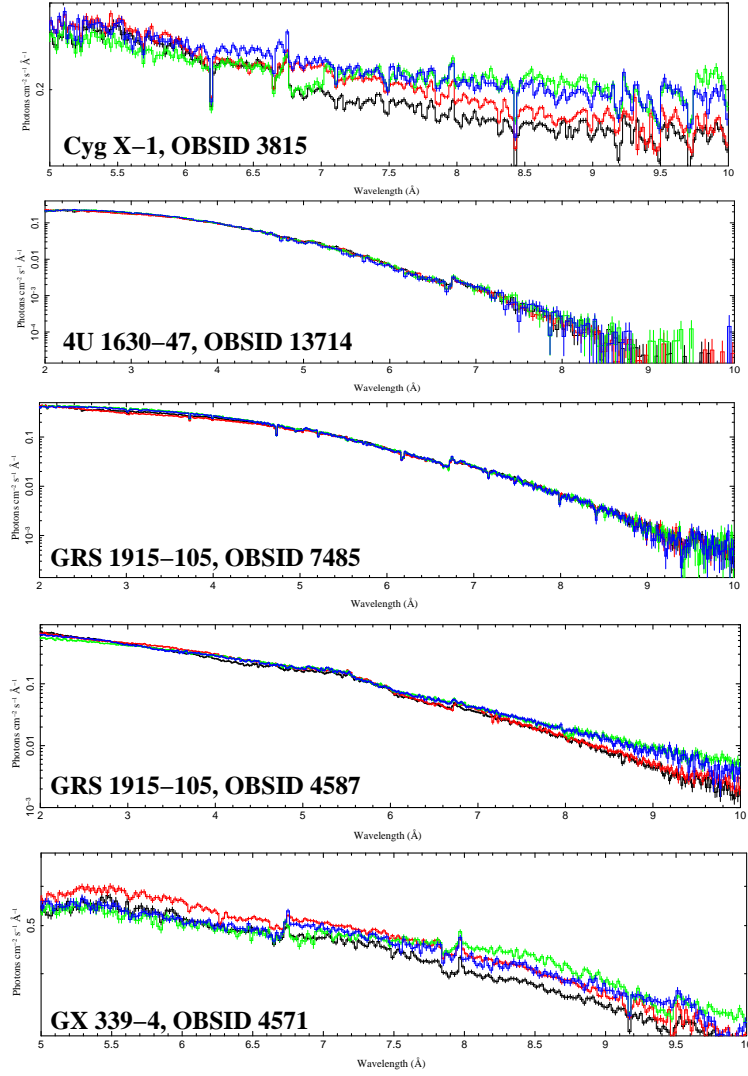


Fig. 8.— Same as Figure 7 but for bright BH sources above 200 mCrab

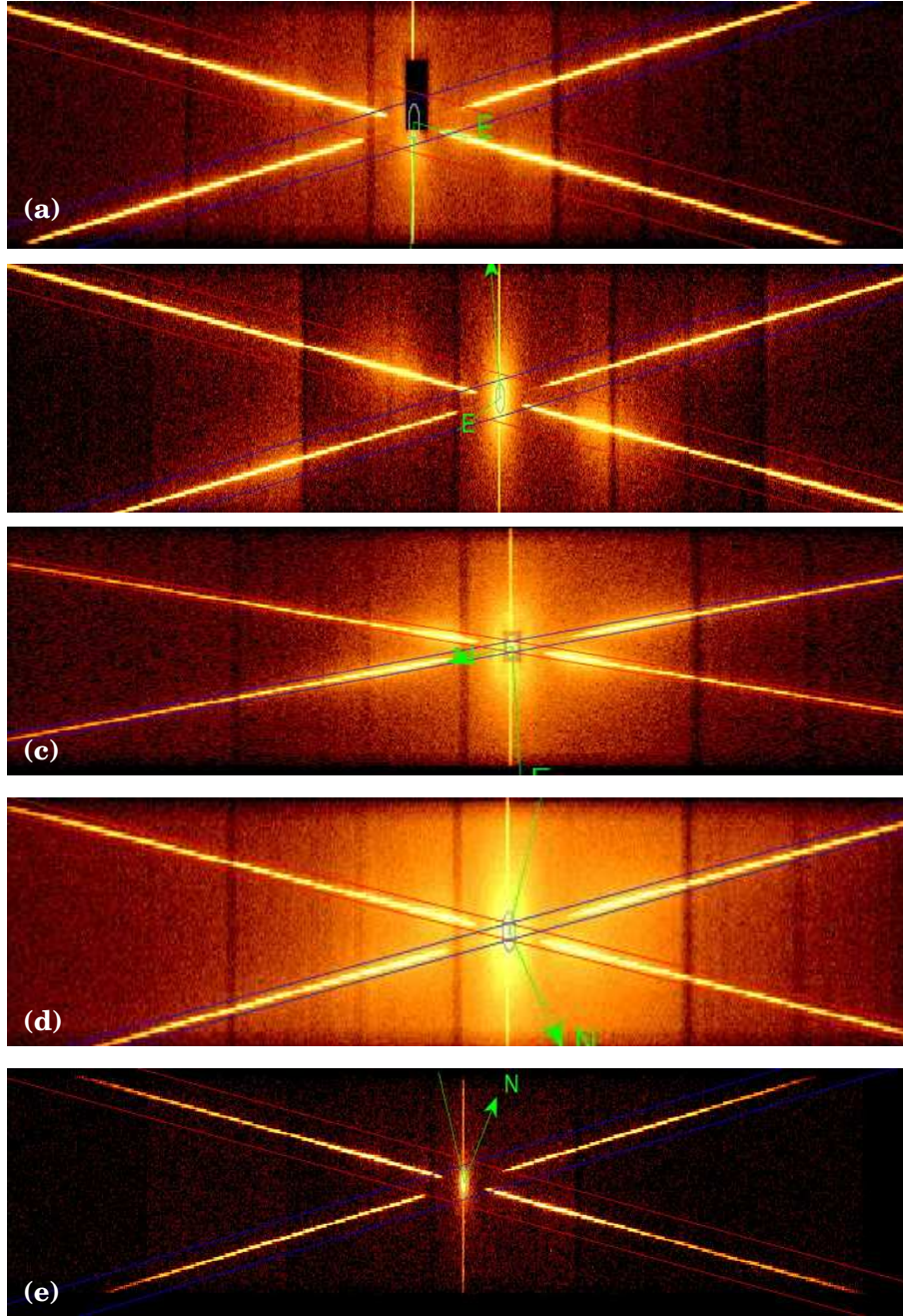


Fig. 9.— Five cases of X-ray scattering halos and its dispersion observed with HETG in TE mode. The colored regions indicate the extraction regions for MEG (red) and HEG (blue) spectra. The green arrow marks the orientation towards the north. The central oval is the zero order extraction region. **(a)** The HETG extraction regions and arrays of Cyg X-2 (~ 450 mCrab) are moderately absorbed with about $3 \times 10^{21} \text{ cm}^{-2}$ column density in the line of sight. **(b)** The same for Cyg X-1 (~ 650 mCrab) at $8 \times 10^{21} \text{ cm}^{-2}$, **(c)** for 4U 1630-47 (~ 200 mCrab) at $1 \times 10^{23} \text{ cm}^{-2}$, **(d)** GRS 1915+105 (~ 400 mCrab) at $5 \times 10^{22} \text{ cm}^{-2}$. **(e)** is the calibration source 4U 1957-115 (~ 35 mCrab) at $1 \times 10^{21} \text{ cm}^{-2}$.

calibration source 4U 1957-115, which has a flux of 35 mCrab and an absorption column of about $1.5 \times 10^{21} \text{ cm}^{-2}$. Even though the X-ray source is relatively soft, the source has low enough absorption to not produce a significant dispersed overlapping scattering halo. Consequently the HETG spectral arms agree well in the specified bandpass in TE and CC-mode as shown in Figure 6.

This appearance changes dramatically in sources with higher flux and absorption. Panels a - d in Figure 9 shows four examples. As dramatic as these pictures appear, however, not all of the bright diffuse emissions actually affects the dispersed spectra of the point source because of the order sorting in PHA space, which excludes much of the diffuse emission. An example is a comparison of panels c and d, which has corresponding HETG spectra in Figure 8, OBSID 13714 and 4587, respectively. While the spectra in OBSID 13714 show little diversity, the ones in OBSID 4587 do, even though the sources are similarly bright and absorbed. However, the source spectrum in OBSID 13714 is very hard, it drops over three orders of magnitude in the specified bandpass, while the one in OBSID 4587 drops less than two orders of magnitude. In sources such as in Cyg X-2, Cyg X-1, GX 339-4 (see Figures 7 and 8) spectra are very flat and soft and even though absorption does not appear as high, its dispersed halo spectra produce visible distortions. How sensitive the shape of the source spectrum is for this issue can be seen in the two spectra shown for GRS 1915-105 (see Figure 8). While in OBSID 7485 the spectrum drops again rapidly allowing for the OSIP PHA window to be a much more effective filter and thus CC-mode obstruction effects are comparatively small, in OBSID 4587 the spectrum of the same source is now much flatter and obstruction effects including MEG higher order overlaps (see below) have a much more significant effect on the measured spectra.

Figure 10 attempts to illustrate the effect of a dispersed scattering halo plus other effects (see below) on the extracted source spectrum. The spectrum of the scattering halo is usually soft and affects spectra below about 3 keV. However the exact shape of the spectrum is unknown and is part of extensive science investigations. Spectra can be affected above about 3 keV depending how much the Si K and maybe even the S K edges are compromised. The top panel simply illustrates how the source image consisting of a point source and a scattering halo disperses in MEG and HEG and which CCDs are primarily occupied. The middle two panels then show how the actual source spectrum gets distorted by spatial overlaps in the collapsed dispersed halo spectrum. The resulting smear in the halo spectrum then comes from the fact that the gratings in HETG are inclined with respect to the readout direction. A large fraction of halo events overlap with the OSIP extraction window and add to the actual source spectrum. Together with CC-mode backgrounds, a different treatment of the Si K edge in FI and BI devices, and MEG higher order overlaps in the HEG, the actual source spectrum gets distorted in different ways for each spectral grating arm. This

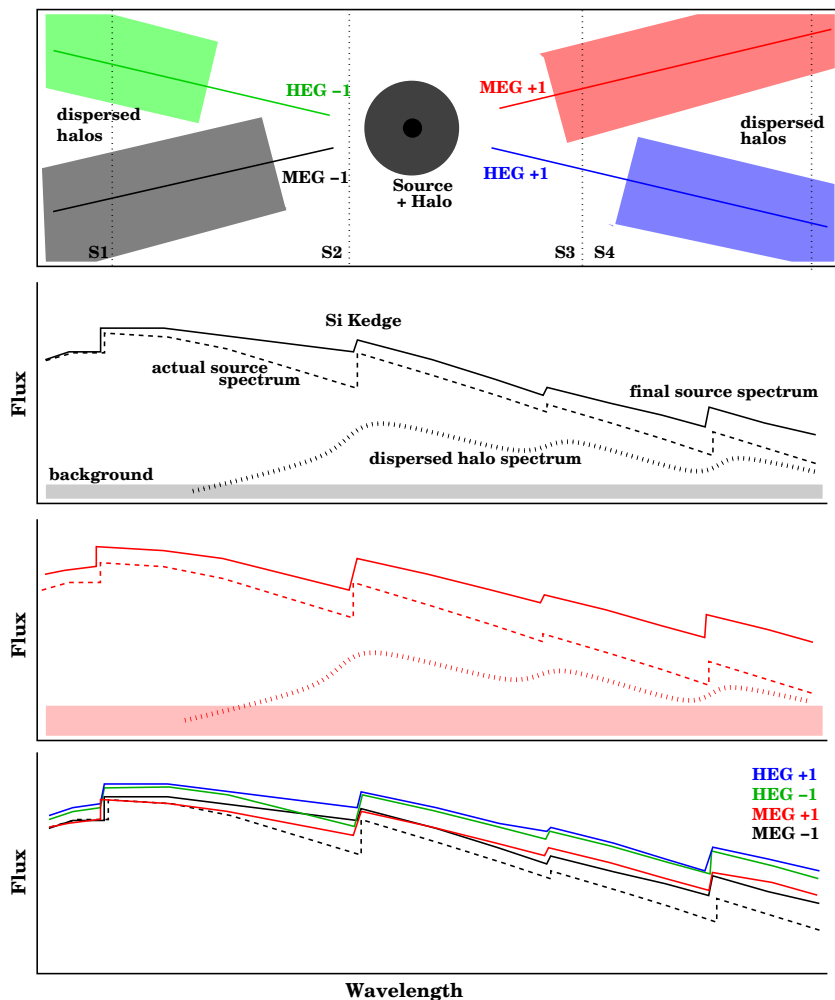


Fig. 10.— A sketch illustrating the effect of various spectral obstructions to the extracted dispersed source spectrum due to collapsed dispersed images in CC-mode. At the foremost a spectral overlap at soft X-rays due to a collapsed dispersed halo spectrum. The top panel illustrates the image effect, the middle two panels the effects on the MEG -1^{st} (black) and MEG $+1^{st}$ (red) spectra. While the soft halo spectrum is likely very similar, there are different CC-mode backgrounds and Si K edge modifications. In the MEG $+1^{st}$ order the Si K edge is least affected since it falls on a BI (S3) device. The bottom spectrum shows all four HETG spectral arms on top of each other with respect to the actual point source spectrum (dashed line). Here the HEG spectra, HEG -1^{st} (green) and HEG $+1^{st}$ (blue) also appear systematically higher in the soft range because of MEG higher order overlaps. The HEG -1^{st} spectrum also is less modified at the Si K edge because it falls on a BI (S1) device

is illustrated in the bottom panel of Figure 10 which show all modified spectral arms with respect to the actual source spectrum.

Such an extended halo dispersion can be modeled using MARX. Figure 11 shows such for Cyg X-1 indicating the order overlap of point source and halo. The effects of the dispersed scattering halo in general depends significantly on the shape of the source spectrum as well as the spectrum of the scattering halo itself. Depending on both shapes the actual source spectrum in the HETG orders are either insignificantly affected or grossly distorted. Should the latter be the case, the determination of the actual source spectrum in HETG CC-mode spectra requires detailed modeling of the interstellar scattering halo spectrum. The observer then needs to model interstellar X-ray scattering which is a foremost consequence of the line of sight composition, density, and abundance of the interstellar medium and thus a difficult science project.

5.1. The Si K and other edges

The illustration in Figure 11 also indicates that photoelectric absorption edges are also affected by the halo dispersion. The scattering halo spectrum also has photoelectric absorption edges naturally from the same line of sight. However, as also indicated, because of the slight inclination of the gratings toward the readout, these edges have a slight smear as well as different optical depths depending upon the scattering medium. This will affect at least the measured optical depth in the edges of the actual source spectrum and likely lead to a decrease in the measured value for all the edges that appear in the halo spectrum. Which ones at the end appear and at which depth has to be modeled. Figure 12 shows a MARX simulation (courtesy of J. Lee et al.) for GRS 1915+105 and Si K. In the case of a single point source simulation the outcome of CC- and TE-mode should be the same, not accounting for the slight smear effect. However, once the simulation adds additional extended emissions, the CC-mode case records a significantly lower optical depth. In the case of GRS 1915+105 the effect is expected to be extreme because of the expected intrinsic dusty environment of the X-ray source and accounts for an almost 40% loss in optical depth. We estimated from Si K edges of many other X-ray binaries using TE versus CC-mode data that effects will amount to between 5 and 20%.

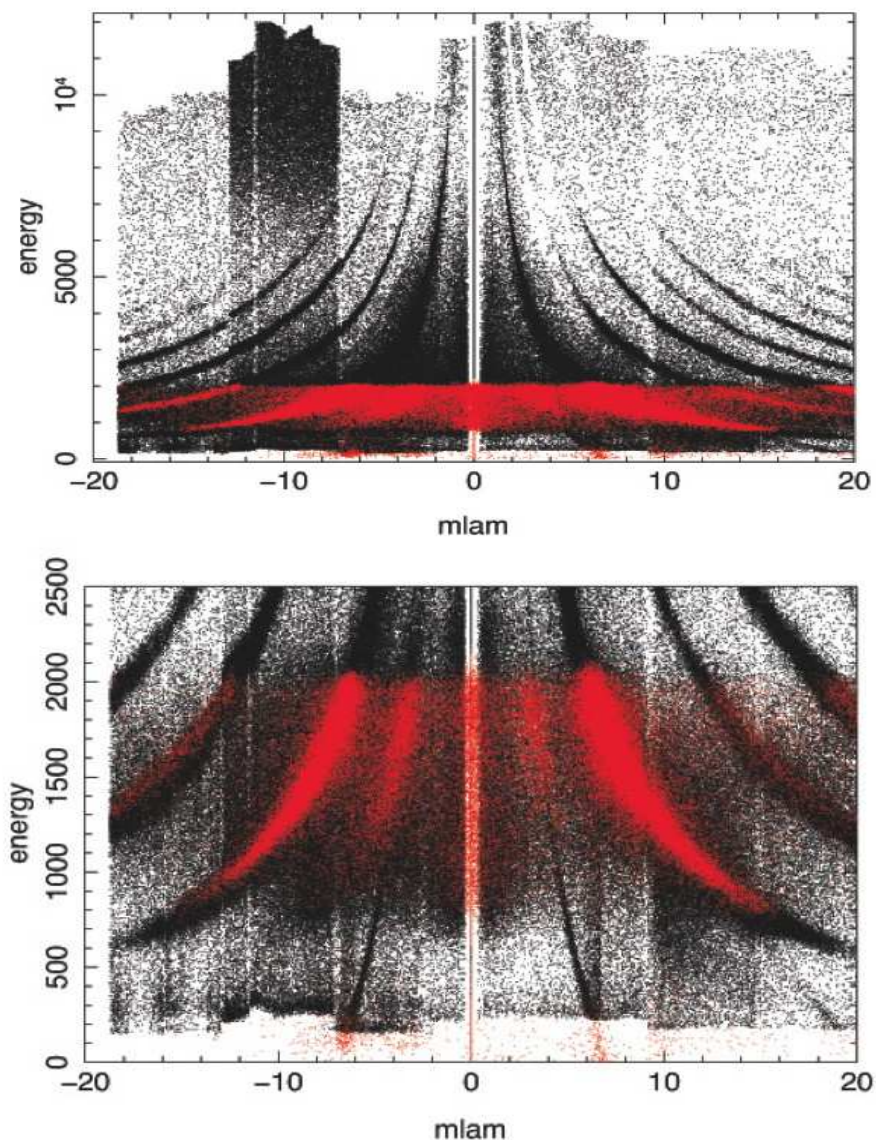


Fig. 11.— MARX simulation for the case of Cyg X-1 in a configuration where one MEG and one HEG spectral arm were kept off the CCD array. The black points are from a typical Cyg X-1 point source spectrum, the red points are from a halo spectrum below 2 keV. The two panels show the resolved events for HEG minus (left side) and MEG plus (right side) orders for the full available energy scale. The bottom panel is limited to 2.5 keV. In the simulated case the halo spectrum fully overlaps with the HEG -1st and MEG +1st orders creating the mismatches of the spectra such as observed in Figure 8 top panel. In other words, the halo spatial extent maps to a width in tg_mlam greater than that of the point source.

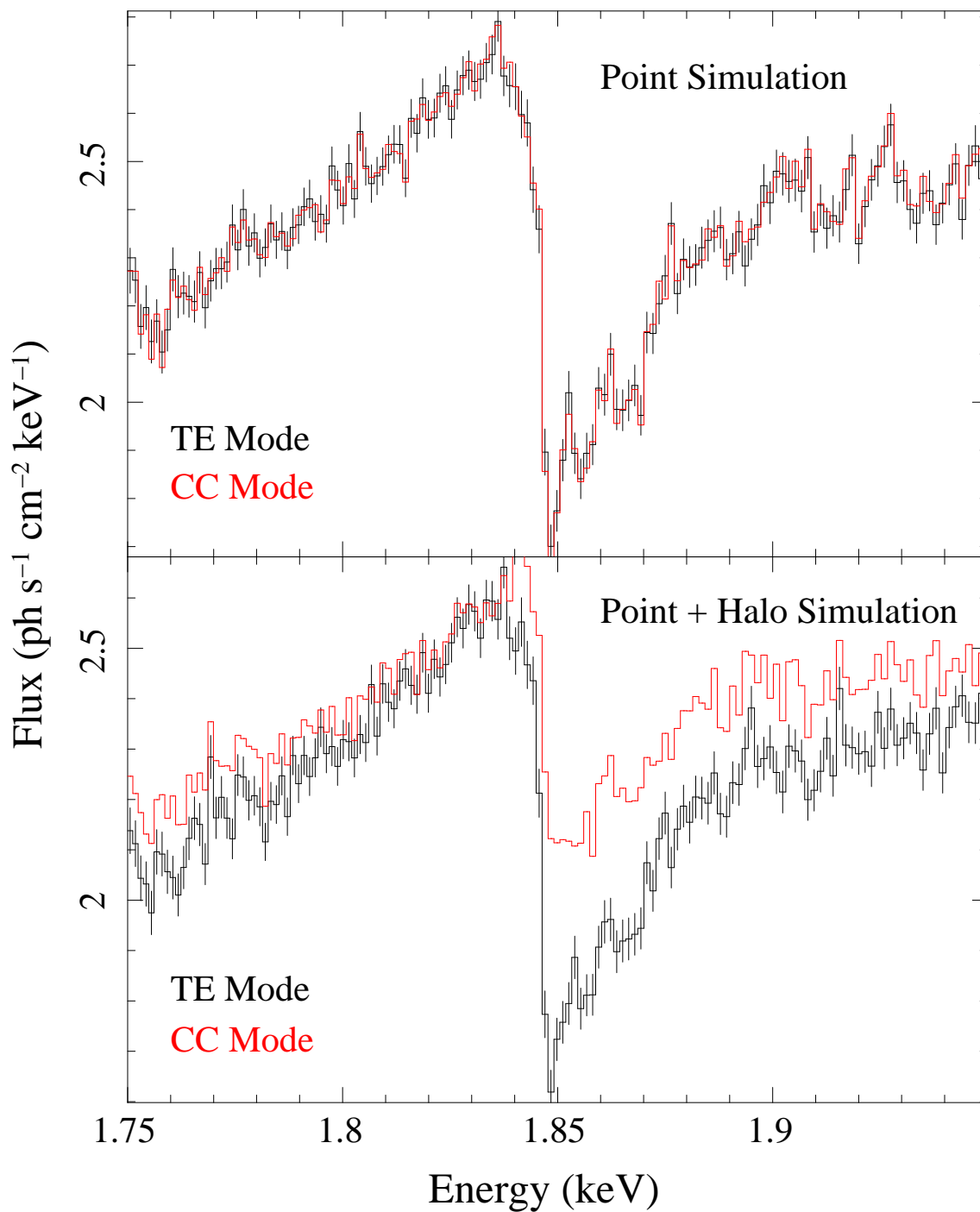


Fig. 12.— Marx simulation of a Si K edge for the case of GRS 1915+105. The top figure shows the case where the X-ray source is a single Chandra point source dispersing the standard Chandra point spread function (psf), the bottom figure adds a flat scattering halo to the psf which in the case of CC mode gets collapsed into the extracted HETG spectrum.

5.2. Si K edge Overcorrection in FI Devices

The Si K edge in the HETG CCD array is a specifically complex issue because while the BI device is thinner, has a more transparent gate structure, and is illuminated from the backside, its quantum efficiency function does not feature much intrinsic Si K absorption. This is different in front illuminated devices, where X-rays have to penetrate a substantial layer of SiO₂. Figures 13 to 15 show how this manifests itself in CC-mode data around the Si K edge for the cases of low and high absorption columns in the bright binaries Cyg X-2 and 4U 1728-34. While in the case of Cyg X-2, which has a low column, the Si K edge in the MEG +1 and HEG -1 orders is clearly visible and its optical depths are of the order of its expected value, in the MEG -1 and HEG +1 orders it either does not exist or even an excess appears. The reason for this behavior lies in the nature of the CCD devices in the array. The previous cases both fall on BI devices, the latter cases are on FI devices. Since BI devices do not need an instrumental Si K correction, its absorption column is high enough and the source is bright enough to produce a measurable edge at Si K, only affected by the extended halo dispersion. The FI edge is also affected by the halo dispersion; however while the halo corrected part gets blurred and thus the applied correction is slightly off, the source part still gets corrected properly. This combination can lead to an imprint of the instrument correction function as observed in Figure 14 in the left panel, where the residuals clearly indicate the SiO₂ transmission features in the data. This effect is only visible as such where the source Si K edge optical depth is low enough to be statistically comparable to the halo fill rate. Such sources include Cyg X-2, 4U 1828-30, and GX 339-4.

In sources with high Si K depth from the absorption column this effect appears less subtle in that one observes the edge depths on BI devices to be larger and much closer to the expected values, while in FI devices the edges are more blurred and appear with less optical depths. Independent of whether the absorbing column is low or high, the effect again has to be modelled in the context of an absorption scattering background and is thus part of the science analysis.

5.3. The 5.44 Å Effect

While most of the additional dispersive additions we observe in HETG CC-mode spectra are of broadband nature, there is one local feature that appears in almost all spectra. The feature is a broad but localized excess centered around 5.4 Å (2.3 keV). It appears like broad line emission. The feature appears independent of the CCD array morphology and is likely again related to the spatial dispersion features. Evidence for that is that it appears in MEG and HEG at the same location not only in the 1st orders but also in higher order spectra.

We currently have no plausible explanations for the effect and we are trying to reproduce the feature through MARX simulations. Due to its dispersive nature, we again strongly suspect some connection with the halo effect.

6. CC-Mode Backgrounds

There are two background components to consider in CC-mode observations using the HETG. First there is a clocking background which essentially is the standard TE-mode CCD background multiplied by the number of clocking rows, i.e. 1024 pixels plus a contribution from the framestore. The other components are related to HEG spectra and stem from a higher MEG order spectral overlap. Figure 16 shows two examples.

6.1. Clocking Background

This background component arises naturally based on the existing CCD background. In TE-mode observations the background in each pixel is very low and negligible for most HETG spectra. It becomes important in CC-mode as it gets amplified by about a factor 10^3 due to the inclusion of all CCD rows. The background rates are chip-dependent and thus the impact on the four grating arms will be different on the ACIS S-array. This accounts for some of the divergence observed in MEG and HEG +/- orders in Figures 7 and 8. The rates are also slightly energy dependent and some of the rates per second and CCD are listed in every years Proposers Observatory Guide.

The largest differences in rates are between BI and FI devices and this makes the background contribution discontinuous in HETG dispersion direction. In order to model this background component one thus has to include the aspect solution which should be done with MARX in sync with the halo modeling. Commonly one can also try to extract this background also in the PHA order sorting window, which is described in Sect. *Future Observation Guidelines* below. In most cases it might be sufficient to account for the contribution at low energies (high wavelengths) only since here most spectra become fainter and background is statistically more significant. In that case one might simply subtract a flat rate corresponding to the FI/BI rates in each spectral arm. Extraction of this background can be done by selecting pulse heights in between orders as indicated in Fig 2 (green box) for the MEG +1 first orders.

6.2. High Order Background

The TE-mode order sorting in HETG observations relies on spatial and CCD spectral separations of MEG and HEG and their higher orders. MEG and HEG spectra are spatially separated and once extracted the CCD PHA space separates the higher order very effectively. In CC-mode this is no longer the case as here MEG and HEG are no longer spatially separated and their orders can overlap in CCD PHA space.

This can be seen in Figure 2. In standard CC-mode observations the OSIP blanks out the MEG even orders during extraction, however physically the even order counts are still recorded. This cannot be changed and it means that counts from mostly the the MEG 2nd orders will overlap into the HEG 1st order. Other overlaps are unlikely in PHA space due to the dispersive nature of the gratings. The MEG second order efficiencies are about 5% to 10% depending on bandpass. In order to account for this overlap HEG 1st order spectra should then have multiple responses assigned: HEG 1st order and MEG 2nd order.

7. Future Observation Guidelines

Observations of very bright X-ray sources with the HETG in CC mode in most cases require careful choices of configurations and modes as well as background subtractions and spectral modeling. The following summarizes a few suggestions that the observer and analyst can follow in order to successfully extract and model the X-ray source spectrum in the HETG gratings.

7.1. Configurations

There are various configurations one can choose to mitigate either pileup in TE mode or background and imaging effects in CC mode. While the choice of subarrays in TE proves to be an effective tool in most cases, such a choice is not available in CC mode. Two configurations are being considered. The first is the standard configuration with all four grating arms on the CCD array. In this case the zero order should be moved as close as possible towards the readout of the CCD to optimize order sorting and allow for sufficient PHA space in between orders for efficient background extraction (see below).

The second configuration puts two grating arms off the CCD array, i.e. moves the zeroth order right next to the first readout row. This is shown at the bottom of Fig. 1. Even though this comes at the expense of about half of the maximum exposure, such a configuration has

several advantages. The first advantage is that it eliminates the higher order background in the HEG as the corresponding MEG orders are off the CCD array. It also eases the standard background extraction as HETG orders remain well separated at all times. It also has great advantages with respect to the modeling of the effect of the scattering halo and the dispersion of the psf scattering wings. In this case only parts of the dispersed zero order image components make it on the array, edges in the spectra are much less affected, and the spectra in orders are in much better agreement. Last but not least, in this configuration both Si K edges can be put onto BI devices. For this a Y-offset of about +1 arcmin needs to be applied from the nominal aimpoint. In general this configuration will greatly ease the modeling effort.

7.2. Background/Halo Extraction

There are several ways to extract the standard CCD background. Basis for the extraction is the order sorting in pha space as shown in Fig. 2. The background is extracted from the spaces in between the orders as indicated by the green regions for the case of the MEG +1st order. To date there is no specific tool available to do the extraction and currently one has to do it manually.

However there is a *vwhere* tool for the use in *ISIS* in the testing phase. The tool *bsub* allows one to extract backgrounds in between orders on an interactive basis. Key here is to efficiently exclude all source photons in the the OSIP extraction and normalize the remainder to the excluded source area. An example of such an extraction is shown in Fig. 17. The blue polygon contour in the left panels is the chosen envelope for all the source counts within the OSIP extraction window. The count spectra in the right panel are the corresponding background extractions. In the case of the 4U 1957+115 the background contributes up to about 5% to the total spectrum. The backgrounds in Fig. 17 appear to have only a slight dependence on wavelength and some dependence on CCD location. The background appears continuous because of the telescope dither. The background levels are higher than predicted from the POG standard CCD background values once normalized to CC-mode and the chosen extraction regions which is expected due to some contributions from faint source and halo scattering events.

The application of this tool is limited as it does not account for the direct effects of all additional dispersive components on the source spectra. It can be useful in cases where additional dispersive components are minimal or when the suggested configuration with two grating arms are off the array is used. Fig. 18 shows an example for such an analysis for the case of Cyg X-1 in a CC-mode observation with this configuration. Here MEG +1st and

HEG -1st orders are available and after correcting for the extracted background both are in quite reasonable agreement. However, there is still a residual systematic effect of the edge modifications to be considered in the final analysis.

7.3. Modeling

In most cases all additional spectral components that are present in CC-mode HETG spectra need to be modeled during the science analysis. This also includes the standard CC-mode background for the simple reason that it is merged into the other dispersive imaging components. At this point there is yet no example available but one will be provided at a later stage. For now the observer should utilize *MARX* to model the dispersion of the source scattering halo, apply the full energy dependent point spread function with its dispersion of the core plus scattering wing, and the distribution of the standard CCD background.

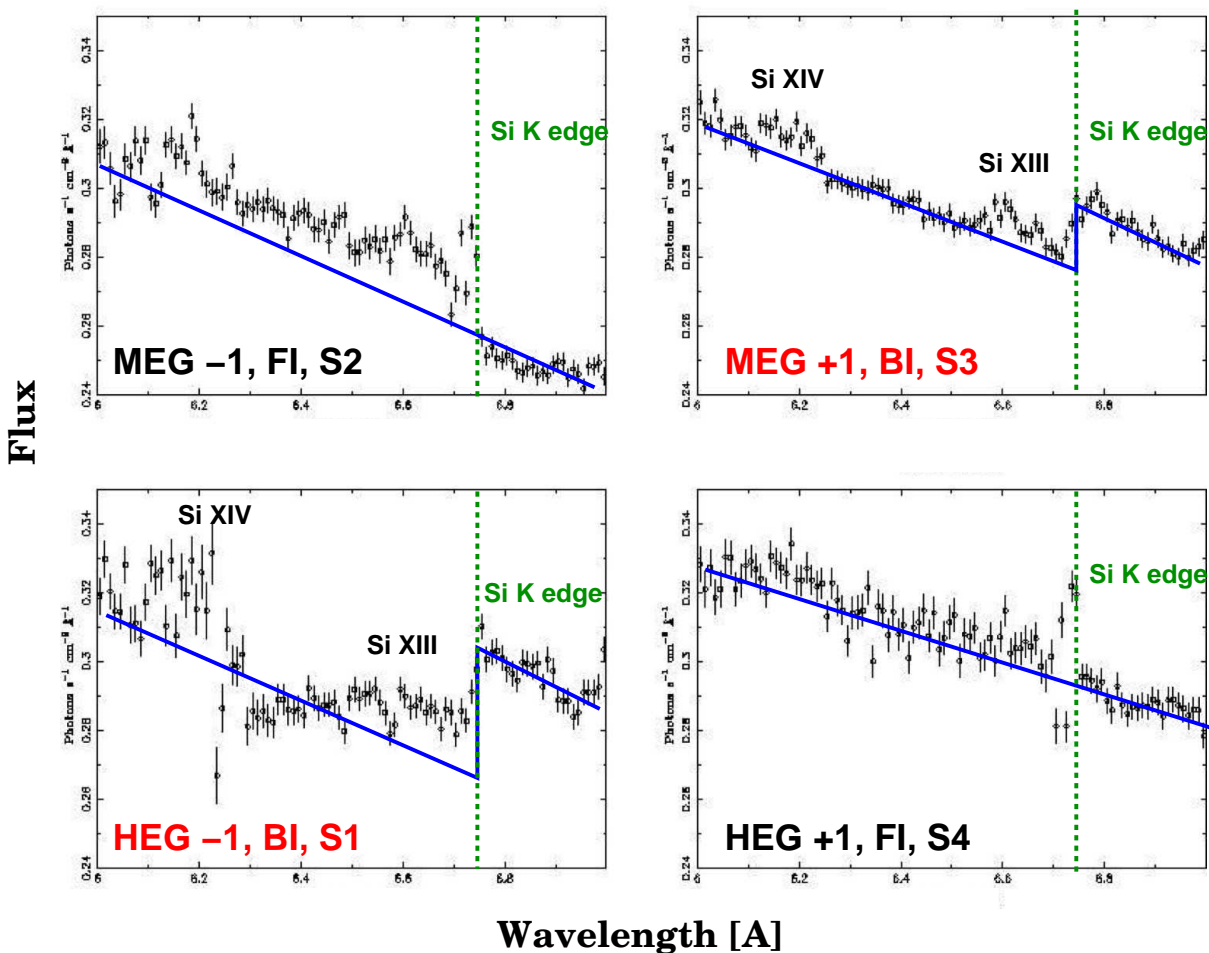


Fig. 13.— Appearance of the Si K edge in all four spectral arms of the \pm 1st order in MEG (top panels) and HEG (bottom panels) for Cyg X-2 in CC mode, which has an absorption column of around $3 \times 10^{21} \text{ cm}^{-2}$. The blue line marks how a local fit picks up the Si K edge, which is recognized in BI devices, but not in FI devices, where it gets overcorrected. As one of the consequences, ionized lines such as Si XIV and Si XIII are only seen in BI devices. The Si K edge in BI devices also appears to not drop sharply indicating the smear from extended image photons.

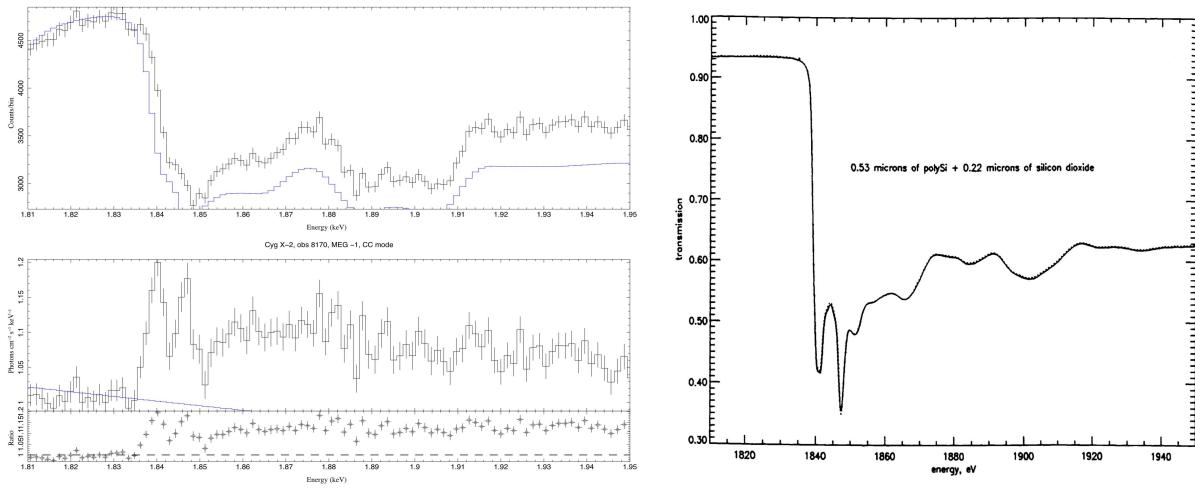


Fig. 14.— **Left:** The Si K edge in Cyg X-2 on a FI device. Due to the edge fill of the scattering background the Si K instrument correction gets imprinted into the residuals. **Right:** The SiO₂ transmission function measured for FI devices in ground calibration.

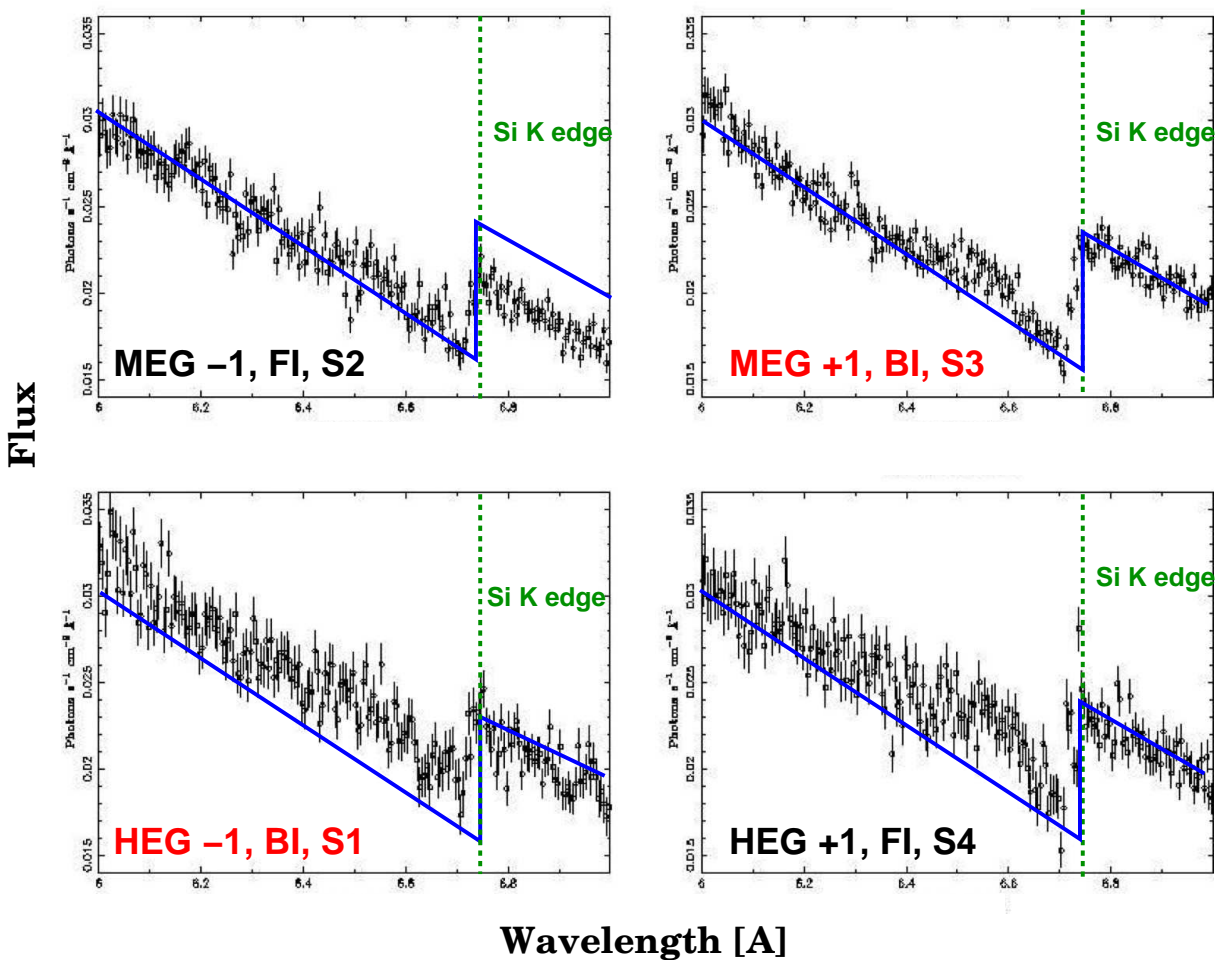


Fig. 15.— Appearance of the Si K edge in all four spectral arms of the ± 1 st order in MEG (top panels) and HEG for 4U 1728-34 in CC mode, which has an absorption column of around $2.5 \times 10^{22} \text{ cm}^{-2}$. Here the blue line indicates how a fit to the MEG +1st data of S3 transposes on the other spectral arms.

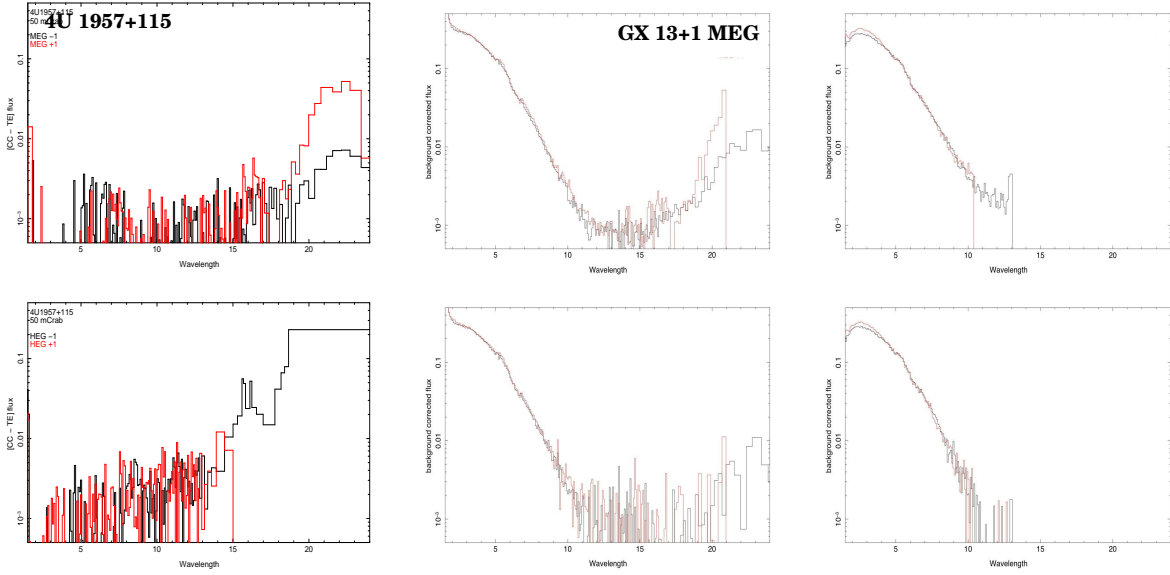


Fig. 16.— Background correction from data. **Left:** Difference spectra for 4U 1957+115 between TE and CC mode observations. These difference spectra account for all the backgrounds between TE and CC-mode. **Middle:** Application of these background spectra to GX 13+1 for the MEG +1st (red) and -1st (black) orders. The top panel is the uncorrected data, the bottom with the background data applies. **Right:** Same for HEG -1st (red) and +1st (black) orders.

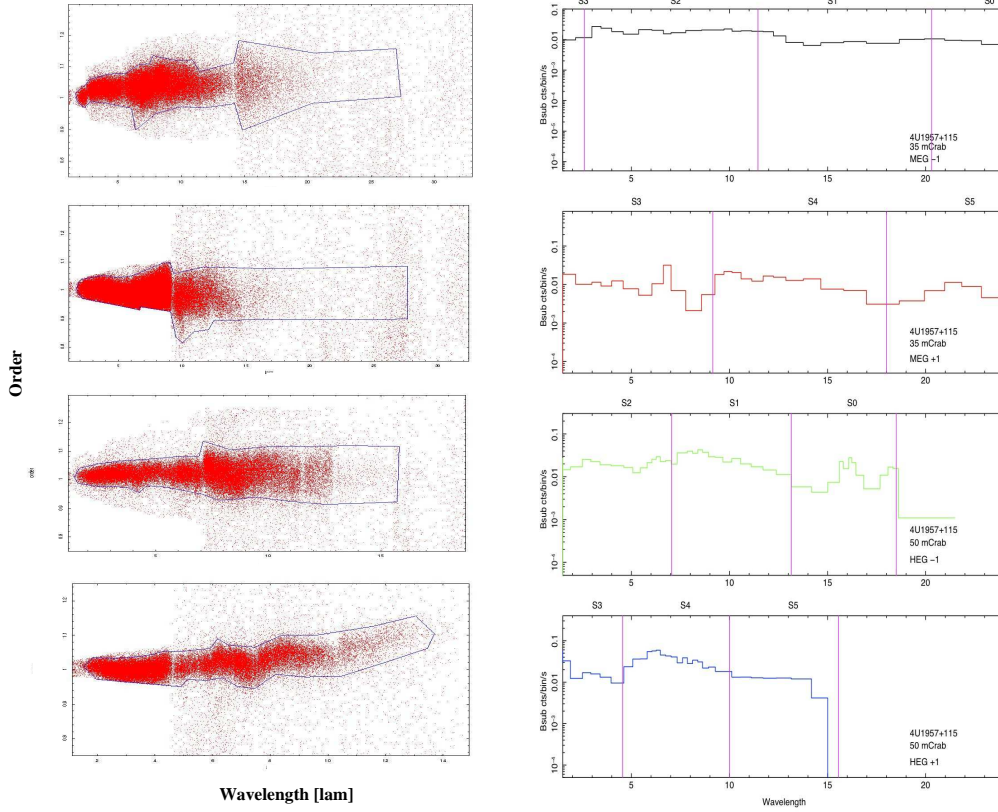


Fig. 17.— Background extraction from data. **Left:** PHA extraction regions using the order sorting plot for the 4U 1957+115 CC-mode observation (OBSID 10660), MEG -1st, +1st, HEG -1st, +1st from top to bottom. **Right:** The corresponding extracted background spectra in the same order. The CCD boundaries are approximate as they dither smeared, which also makes the background spectra look fairly continuous.

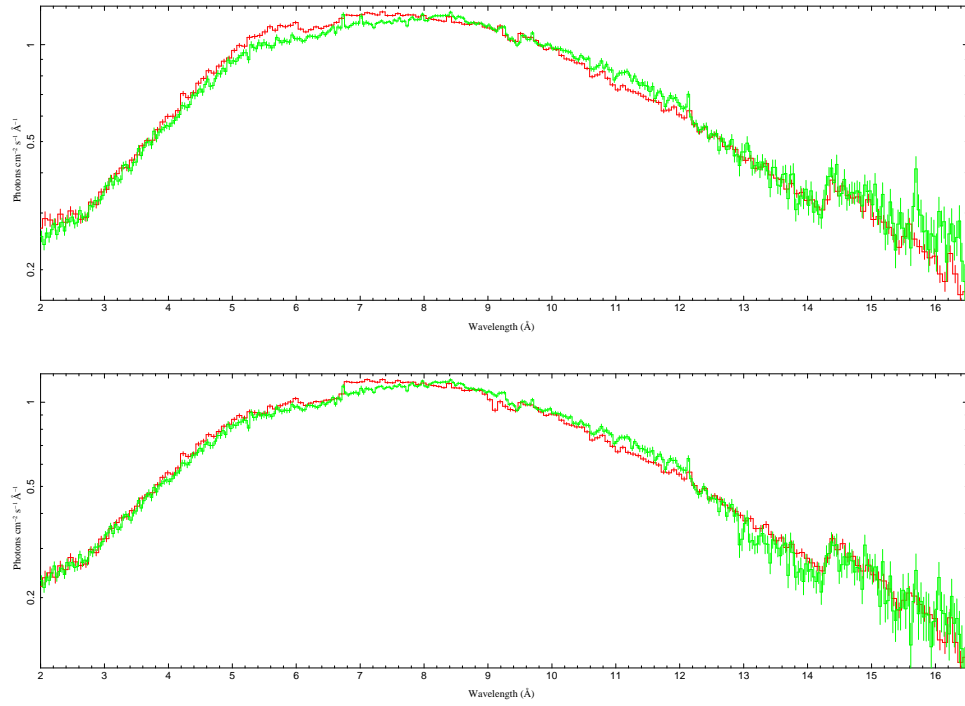


Fig. 18.— Background/halo subtraction from Cyg X-1 data in the suggested CC-mode configuration placing two grating arms off the CCD array (place holder)